

Dual-Tree Cosine-Modulated Filter Bank With Linear-Phase Individual Filters: An Alternative Shift-Invariant and Directional-Selective Transform

Lili Liang and Han Liu

Abstract—Dual-tree transforms have recently received much attention for the properties of shift-invariance and directional-selectivity. However, their designs generally encounter fractional-delay constraints, and become more complicated for providing linear-phase (LP) individual filters and flexible directional-selectivity, two important properties in image processing. In this paper, we propose an alternative shift-invariant and directional-selective transform—the dual-tree cosine-modulated filter bank (DTCMFB). In the proposed DTCMFB, its primal and dual filter banks are derived by cosine-modulating one LP prototype filter, and thus its design involves no fractional-delay constraints. Meanwhile, the derived modulation technique guarantees each individual filter to be LP and the LP condition is satisfied without any constraint on the prototype filter. By separable operations, the DTCMFB is extended to two-dimensions. The resulting 2D DTCMFB can provide much more flexible directional-selectivity. Finally, several simulations are given to verify the proposed DTCMFB, and the experiments on nonlinear approximation and image denoising are presented to demonstrate its potential in image processing.

Index Terms—Cosine-modulation, directional-selectivity, fractional-delay constraint, linear-phase, shift-invariance.

I. INTRODUCTION

IT IS well known that the use of discrete wavelet transform (DWT), due mainly to the lack of shift-invariance and directional-selectivity [1], is hampered in many signal/image processing applications, such as image denoising and feature extraction. For solving the two problems, the dual-tree complex wavelet transform (DTCWT) as shown in Fig. 1(a) was introduced [2] and then discussed theoretically [3]–[5]. It is constructed by two parallel critically-decimated filter banks (FBs) and has the limited redundancy of 2^d for d -dimensional signals, which is independent of decomposition level. By constraining the aliasing caused by downsampling in the primal FB to be cancelled approximately with that in the dual FB, the DTCWT achieves approximate shift-invariance and

Manuscript received August 6, 2012; revised January 25, 2013; accepted September 9, 2013. Date of publication September 23, 2013; date of current version October 4, 2013. This work was supported in part by the National Science Foundation of China under Grant 61174101, in part by the Ph.D. Programs Foundation of the Ministry of Education of China under Grant 2012611811004, and in part by the Doctor Research Start Fund of Xi'an University of Technology under Grant 105-211307. The associate editor coordinating the review of this manuscript and approving it for publication was Prof. Ton Kalker.

The authors are with the Department of Automation and Information Engineering, Xi'an University of Technology, Xi'an 710048, China (e-mail: liliang@xaut.edu.cn; liuhan@xaut.edu.cn).

Digital Object Identifier 10.1109/TIP.2013.2283146

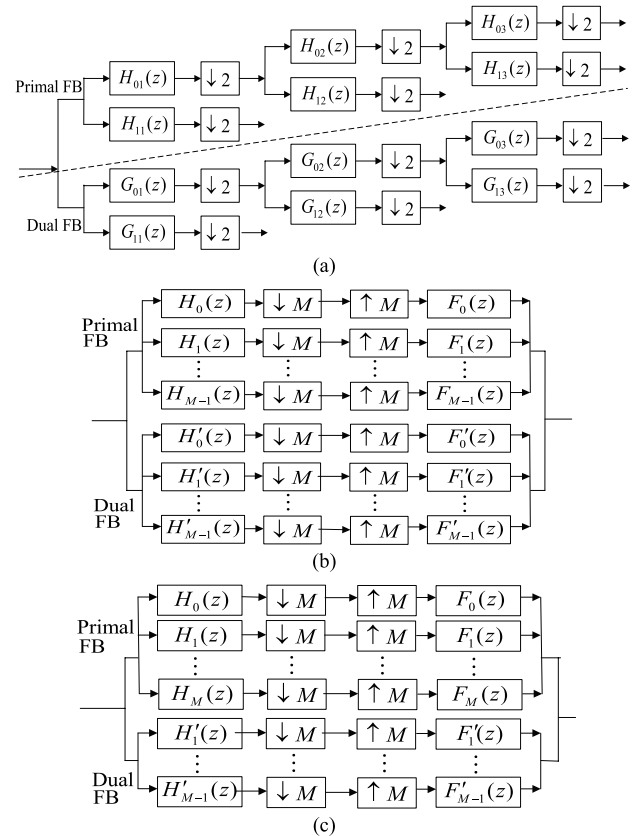


Fig. 1. Structures of dual-tree transforms. (a) DTCWT (analysis part) [2], (b) M-band DTCWT [6] and CSMFB [18], (c) DOECFB [19].

six directional subbands in two-dimensions. Actually, the ‘six’ directions are insufficient to represent images with abundant directional features. To offer more choice of orientations, Chau, Duval and Pesquet generalized the DTCWT from two-band to M -band ($M > 2$) as shown in Fig. 1(b) [6]. Besides shift-invariance and low redundancy, it provides $2(M^2 - 1)$ directional subbands in each decomposition level. Later, the DTCWT [2] was extended to the dual-tree complex wavelet packet (DTCWP) by iterating certain FBs on the low-pass and high-pass outputs of both the primal and dual FBs [7], resulting in $2(2^L - 1)$ orientations for an L -level decomposition. Inspired by the idea of DTCWT, some other shift-invariant and directional-selective transforms including the double-density dual-tree DWT [8], shiftable complex directional pyramid

[9], [10], Gabor-like wavelet [11], and the non-redundant complex wavelet transform [12] were proposed.

These dual-tree transforms (DTTs) indeed gave better performances in some applications [13]-[16]. However they have to encounter two limitations. One is the fractional-delay constraints. That is, for ensuring the aliasing in the primal and dual FBs to cancel each other, the scaling filter of the dual FB in DTCWT or DTCWP has to be the half-delayed version of that of the primal FB. This problem becomes more serious in the M -band DTCWT [6], since it imposes the fractional-delay constraints not only on the scale filters, but also wavelet filters. Up to now, there exists no efficient time-domain method for designing the FIR-based M -band DTCWT ($M > 2$) [6]. The other limitation that should be pointed out is that their analysis/synthesis filters are difficult to have linear-phase (LP) property which is of great importance in image processing. Besides allowing simple symmetric extension methods to handle the boundary of finite-length signals [17], the LP filters can eliminate the phase distortion and preserve the edge information of images. However, the fact is that the DTT designs will become more complicated when imposing LP constraint on each individual filter.

In response to the limitations above, the cosine-modulation was introduced into designing DTTs [18], [19]. In [18], the cosine-sine modulated filter bank (CSMFB) which has the same structure as in Fig. 1(b) was developed by taking the cosine-modulated and sine-modulated FBs [20] as the primal and dual FBs, respectively. Although the CSMFB avoids fractional-delay constraints, its modulated analysis and synthesis filters cannot have the LP property theoretically. In [19], the proposed delay-less oversampled even-stacked cosine-modulated filter bank (DOECFB) arose from the LP critically-decimated ECFB [21] by replacing the decimation factor $2M$ with M (see Fig. 1(c)), and thus has the LP individual filters. However, it is at the cost of constraining the prototype filter order N to be $(2m_0 + 1)M$, where m_0 is a positive integer. This constraint together with its perfect-reconstruction (PR) condition requires that the prototype filter must have $2m_0 + M - 1$ zero coefficients for odd M and $4m_0 + M - 1$ for even M . These zero coefficients will reduce the prototype filter quality especially when M is even. Further, from Fig. 1(c) it can be seen that, the primal lowpass and highpass filters have no corresponding dual filters. This will mix some directions together and reduce the efficiency of image representation.

In this paper, we propose a new cosine-modulation based DTT, which is named the *dual-tree cosine-modulated filter bank* (DTCMFB). In the proposed DTCMFB, both the primal and dual FBs are designed by cosine-modulating a FIR prototype filter, and meanwhile the aliasing appearing in the two FBs can cancel each other approximately. Consequently the design of DTCMFB avoids fractional-delay constraints and is reduced to that of one prototype filter. Further, in order for the proposed DTCMFB to have LP analysis/synthesis filters, we derive the modulation technique for each individual filter, with which the LP condition can be satisfied without any constraint on the prototype filter. It is also proved that this DTCMFB is a PR system in structure. By separable operations,

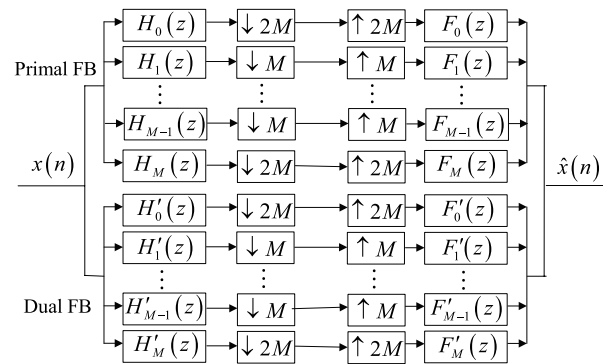


Fig. 2. Structure of the proposed DTCMFB.

the 1D DTCMFB can be extended to two-dimensions, and the resulting 2D DTCMFB can provide much richer directional-selectivity. This is highly desired in directional representation of images.

The remainder of the paper is organized as follows. In Section II, we first propose the structure of DTCMFB and then analyze its shift-invariance conditions. The derivation of LP analysis/synthesis filters of DTCMFB as well as its reconstruction performance is considered in Section III. Section IV analyzes the high directional-selectivity of the DTCMFB in two-dimensions. Several experiments are displayed in Section V to demonstrate the validity of DTCMFB. And we conclude this paper in Section VI. Note that in what follows, we assume that all the involved filters are FIR.

Notations: Lowercase boldface letters indicate vectors and uppercase boldface letters represent matrices. The superscripts T , $*$, and H denote the operations of transpose, conjugation and transpose-conjugation, respectively. \mathbf{I}_k corresponds to a $k \times k$ identity matrix, and $\{\mathbf{P}\}_{k,l}$ denotes the (k, l) -th element of matrix \mathbf{P} . In addition, we define W_M by $W_M = e^{-j2\pi/M}$.

II. CONSTRUCTION OF DTCMFB

In this section, firstly we construct the structure of DTCMFB and make it have the potential to have LP analysis/synthesis filters. Then we analyze under what conditions the proposed DTCMFB will be shift-invariant.

A. Structure of the Proposed DTCMFB

As shown in Fig. 2, the proposed DTCMFB is constructed by two parallel $(M+1)$ -band FBs and thus has the redundancy of 2. In this structure, $H_k(z)$ and $F_k(z)$ denote the analysis and synthesis filters of primal FB, respectively. In a similar way, $H'_k(z)$ and $F'_k(z)$ correspond to the dual FB, $k = 0, 1, \dots, M$. All these filters will be obtained by cosine-modulating one LP prototype filter. In order for each cosine-modulated filter to be LP, we set the bandwidth of bandpass filters to be $2\pi/M$, while that of the lowpass and highpass filters to be π/M . This is because that for a cosine-modulated FB, if all filters have the same bandwidth, they will be hard to achieve LP [21], [22]. Fig. 3 sketches the magnitude responses of the analysis filters $H_k(z)$ and $H'_k(z)$, $k = 0, 1, \dots, M$. The synthesis filters $F_k(z)$ and $F'_k(z)$ have the same magnitude

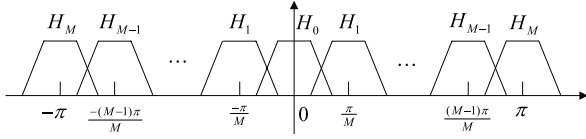


Fig. 3. Normalized magnitude responses of the analysis filters of DTCMFB. Here H_k denotes $H_k(z)$ or $H'_k(z)$, $k = 0, 1, \dots, M$.

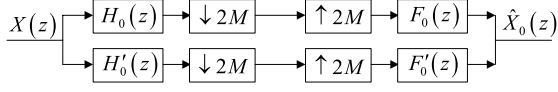


Fig. 4. Lowpass channels of the primal and dual FBs.

responses with their corresponding analysis filters. Further, different from DOECFB in which the primal lowpass and highpass filters do not have dual filters [19], in the proposed DTCMFB, to make each primal filter have a corresponding dual, the decimation factor of bandpass channels is set to be M , while that of the lowpass and highpass is set to be $2M$.

B. Shift-Invariance Conditions

For a DTT, its shift-invariance results from that the aliasing appearing in each channel of primal FB can be cancelled approximately with that in the corresponding channel of dual FB. In the existing DTTs [2]–[9], this is performed by imposing the dual filters to be the fractional-delay versions of the primal ones. In this subsection, we consider under what conditions the aliasing in the primal and dual FBs of DTCMFB can cancel each other approximately. Due to the difference between the lowpass (highpass) and bandpass channels, they will be analyzed separately.

Firstly, we focus on the lowpass channels as shown in Fig. 4. The relationship of the input and output is

$$\begin{aligned} \hat{X}_0(z) &= \frac{1}{2M} \sum_{l=0}^{2M-1} \left[H_0(zW_{2M}^l) F_0(z) \right. \\ &\quad \left. + H'_0(zW_{2M}^l) F'_0(z) \right] X(zW_{2M}^l) \\ &= \frac{1}{2M} \sum_{l=0}^{2M-1} A_{0,l}(z) X(zW_{2M}^l), \end{aligned} \quad (1)$$

The term $A_{0,0}(z)$ in $X(z)$ is linear shift-invariant response, while the terms $A_{0,l}(z)$ in $X(zW_{2M}^l)$, $l = 1, 2, \dots, 2M-1$, correspond to aliasing. In order for (1) to be shift-invariant, those aliasing terms have to be negligible, i.e. $H_0(zW_{2M}^l)F_0(z)$ and $H'_0(zW_{2M}^l)F'_0(z)$ either are small enough or can cancel each other for $l \neq 0$. According to Fig. 3, we know that the shifted filters $H_0(zW_{2M}^l)$ and $H'_0(zW_{2M}^l)$ have the passband $[(2l-1)\pi/2M, (2l+1)\pi/2M]$. By assuming the original filters $H_0(z)$ and $H'_0(z)$ have the stopband edge less than π/M , the passbands and transition bands of shifted filters overlap only with the stopbands of original filters for $l = 2, 3, \dots, 2M-2$ (see Fig. 5). Thus, it is easy to make $H_0(zW_{2M}^l)F_0(z)$ and $H'_0(zW_{2M}^l)F'_0(z)$ small enough by sufficiently attenuating the stopband responses of $F_0(z)$ and $F'_0(z)$. While when $l = 1, 2M-1$, this becomes impossible since

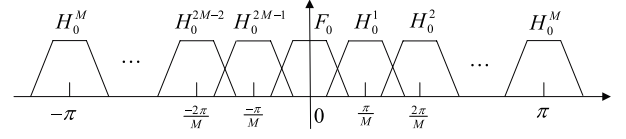


Fig. 5. Sketches of the magnitude responses of $F_0(z)$ and $H_0(zW_{2M}^l)$, $l = 1, 2, \dots, 2M-1$. Here, F_0 denotes $F_0(z)$ and H_0^l denotes $H_0(zW_{2M}^l)$.

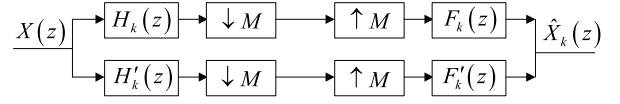


Fig. 6. Combination of the k -th channels of the primal and dual FBs, $k = 1, 2, \dots, M-1$.

$H_0(zW_{2M}^l)$ has a significant transition band overlap with $F_0(z)$ as shown in Fig. 5. Thus, we have to design $H_0(zW_{2M}^l)F_0(z)$ and $H'_0(zW_{2M}^l)F'_0(z)$ to cancel each other for $l = 1, 2M-1$. By defining

$$H'_0(z) = z^{-M} H_0(z), \quad \text{and} \quad F'_0(z) = z^M F_0(z), \quad (2)$$

we derive that

$$H'_0(zW_{2M}^l) F'_0(z) = (-1)^l H_0(zW_{2M}^l) F_0(z). \quad (3)$$

From the above analysis, it is obvious that all the aliasing terms in (1) can be negligible and thus the combination of the primal and dual lowpass channels can have near shift-invariance.

For the shift-invariance of highpass channels, it can be analyzed similarly with the lowpass case by letting

$$H_M(z) = (-z)^{-M} H'_M(z), \quad \text{and} \quad F_M(z) = (-z)^M F'_M(z). \quad (4)$$

Next, we consider the bandpass channels as shown in Fig. 6. It has the following input and output relationship,

$$\begin{aligned} \hat{X}_k(z) &= \frac{1}{M} \sum_{l=0}^{M-1} \left[H_k(zW_M^l) F_k(z) \right. \\ &\quad \left. + H'_k(zW_M^l) F'_k(z) \right] X(zW_M^l), \end{aligned} \quad (5)$$

where $k = 1, 2, \dots, M-1$. According to the discussion on aliasing cancellation of bandpass channels [2], we set

$$\begin{aligned} H_k(z) &= P_k(z) + P_k^*(z), \\ H'_k(z) &= -j [P_k(z) - P_k^*(z)], \\ F_k(z) &= Q_k(z) + Q_k^*(z), \\ F'_k(z) &= j [Q_k(z) - Q_k^*(z)], \end{aligned} \quad (6)$$

where $P_k(z)$ and $Q_k(z)$ are two complex filters, each of which has the single passband $[(2k-1)\pi/2M, (2k+1)\pi/2M]$ and negligible responses at all negative frequencies. Substituting (6) into (5), we rewrite (5) as

$$\begin{aligned} \hat{X}_k(z) &= \frac{2}{M} \sum_{l=0}^{M-1} \left[P_k(zW_M^l) Q_k(z) \right. \\ &\quad \left. + P_k^*(zW_M^l) Q_k^*(z) \right] X(zW_M^l). \end{aligned} \quad (7)$$

Here we assume $P_k(z)$ and $Q_k(z)$ have the lower stopband edge greater than $(k-1)\pi/M$ and the upper stopband edge smaller than $(k+1)\pi/M$. Under this assumption, it can be derived that the passband and transition band of $P_k(zW_M^l)$ overlap only with the stopband of $Q_k(z)$ for $l = 1, 2, \dots, M-1$. Therefore, $P_k(zW_M^l)Q_k(z)$ can also be considered negligible. And so do $P_k^*(zW_M^l)Q_k^*(z)$.

Summarizing, we conclude that if the analysis/synthesis filters satisfy (2), (4) and (6), the aliasing in each primal channel will be cancelled approximately by that in the corresponding dual channel, and thus the proposed DTCMFB will have the property of shift-invariance.

III. DCMFB WITH LP ANALYSIS/SYNTHESIS FILTERS

In this section, we firstly focus on how to derive the LP analysis/synthesis filters of DTCMFB under the conditions (2), (4) and (6), and then consider the reconstruction performance of the DTCMFB with those derived LP filters.

A. Derivation of LP Analysis/Synthesis Filters

As indicated in Section II-A, each individual filter of DTCMFB is a cosine-modulated version of one LP prototype filter. Since the lowpass (highpass) and bandpass filters have different bandwidths, they will be analyzed separately. First of all, we denote by $P(z)$ the prototype filter, which has the passband $[-\pi/2M, \pi/2M]$ and the order N .

According to (2) and (4), we set the analysis lowpass and highpass filters of the primal and dual FBs to be

$$\begin{aligned} H_0(z) &= P(z)/\sqrt{2}, \\ H'_0(z) &= z^{-M}P(z)/\sqrt{2}, \\ H_M(z) &= (-z)^{-M}P(-z)/\sqrt{2}, \\ H'_M(z) &= P(-z)/\sqrt{2}. \end{aligned} \quad (8)$$

Obviously, $H'_0(z)$ and $H_M(z)$ are respectively the integer-delayed versions of $H_0(z)$ and $H'_M(z)$. Thus there is no fractional-delay constraint in (8). Moreover, since $P(z)$ is of LP, each of them has the LP property.

For the analysis bandpass filters $H_k(z)$ and $H'_k(z)$, $k = 1, 2, \dots, M-1$, we first define

$$U_k(z) = P(zW_{2M}^k), \quad (9)$$

and then generate them with (6) as

$$\begin{aligned} H_k(z) &= 0.5(a_k U_k(z) + a_k^* U_k^*(z)), \\ H'_k(z) &= -0.5j[a_k U_k(z) - a_k^* U_k^*(z)], \end{aligned} \quad (10)$$

where a_k is a complex number with unit-magnitude. Denoting a_k by $e^{j\theta_k}$, their time-domain forms can be written as

$$\begin{aligned} h_k(n) &= p(n) \cos\left(\frac{k\pi}{M}n + \theta_k\right), \\ h'_k(n) &= p(n) \sin\left(\frac{k\pi}{M}n + \theta_k\right). \end{aligned} \quad (11)$$

From (11), one can also observe that there are no fractional-delay constraints between the primal and dual bandpass filters.

Further, to make these bandpass filters have LP property, we choose θ_k as $\theta_k = -k\pi(M+N)/2M$ so that $H_k(z) = (-1)^k z^{-N} H_k(z^{-1})$ and $H'_k(z) = (-1)^{k+1} z^{-N} H'_k(z^{-1})$. Obviously with such θ_k , each bandpass filter is of LP. For the synthesis filters $F_k(z)$ and $F'_k(z)$, $k = 0, 1, \dots, M$, we set them as the time-reversed versions of their corresponding analysis filters. Therefore, the synthesis filters also involve no fractional-delay constraints and have the LP property.

By now, all the LP analysis and synthesis filters of DTCMFB have been derived. The impulse responses of primal filters are given below,

$$\begin{aligned} h_0(n) &= p(n)/\sqrt{2}, \\ h_M(n) &= (-1)^n p(n-M)/\sqrt{2}, \\ h_k(n) &= p(n) \cos\left(\frac{k\pi}{M}\left(n - \frac{N+M}{2}\right)\right) \\ &\quad k = 1, 2, \dots, M-1, \\ f_k(n) &= h_k(N-n), \quad k = 0, 1, \dots, M, \end{aligned} \quad (12a)$$

and the dual filters in time-domain are

$$\begin{aligned} h'_0(n) &= p(n-M)/\sqrt{2}, \\ h'_M(n) &= (-1)^n p(n)/\sqrt{2}, \\ h'_k(n) &= p(n) \sin\left(\frac{k\pi}{M}\left(n - \frac{N+M}{2}\right)\right), \\ &\quad k = 1, 2, \dots, M-1, \\ f'_k(n) &= h'_k(N-n), \quad k = 0, 1, \dots, M. \end{aligned} \quad (12b)$$

With the above modulation formulae, one can see that the LP property of each filter is obtained without any constraint on the prototype order N . This is different from the modulation technique in DOECFB [19], which achieves LP filters at the cost of constraining the prototype order to be the odd multiple of decimation factor.

B. Reconstruction Performance

Going back to the structure of DTCMFB as shown in Fig. 2, the relationship between the input and output can be expressed as

$$\begin{aligned} \hat{X}(z) &= \frac{1}{M} \sum_{l=0}^{M-1} \left[\sum_{k=0}^{M-1} H_k(zW_M^l) F_k(z) \right. \\ &\quad \left. + \sum_{k=1}^M H'_k(zW_M^l) F'_k(z) \right] X(zW_M^l) \\ &= \frac{1}{M} \sum_{l=0}^{M-1} A_l(z) X(zW_M^l). \end{aligned} \quad (13)$$

Assume that $\mathbf{E}(z)$ denotes the type-I polyphase component matrices of $[H_0(z), H_1(z), \dots, H_{M-1}(z), H'_1(z), H'_2(z), \dots, H'_M(z)]^T$, and $\mathbf{R}(z)$ is the type-II polyphase component matrices of $[F_0(z), F_1(z), \dots, F_{M-1}(z), F'_1(z), F'_2(z), \dots, F'_M(z)]$. To ensure that there is no distortion between the input and output, that is, the proposed DTCMFB is a PR system, $\mathbf{R}(z)$ and $\mathbf{E}(z)$ have to satisfy [23]

$$\mathbf{R}(z) \mathbf{E}(z) = \mathbf{I}_{2M}. \quad (14)$$

In what follows, we analyze the necessary and sufficient condition for (14) to hold. Firstly we define

$$P(z) = \sum_{n=0}^{2M-1} G_n(z^{2M}) z^{-n}, \quad (15)$$

where $G_n(z)$ is the n -th type I polyphase component of prototype filter $P(z)$, i.e., $G_n(z) = \sum_m p(2Mm+n)z^{-n}$. By using (12) and (15), it can be derived that

$$\mathbf{E}(z) = \begin{bmatrix} \mathbf{C} \\ \mathbf{S} \end{bmatrix} \begin{bmatrix} \mathbf{G}_0(z^2) \\ z^{-1}\mathbf{G}_1(z^2) \end{bmatrix}. \quad (16)$$

$\mathbf{G}_0(z)$ and $\mathbf{G}_1(z)$ are diagonal matrices with $\{\mathbf{G}_0(z)\}_{k,k} = G_k(z)$ and $\{\mathbf{G}_1(z)\}_{k,k} = G_{M+k}(z)$, $k = 0, 1, \dots, M-1$. \mathbf{C} and \mathbf{S} are $M \times 2M$ matrices with the elements below,

$$\begin{aligned} \{\mathbf{C}\}_{0,n} &= 1/\sqrt{2}, \\ \{\mathbf{C}\}_{k,n} &= \cos\left(\frac{k\pi}{M}\left(n - \frac{N+M}{2}\right)\right), \\ \{\mathbf{S}\}_{M-1,n} &= (-1)^n/\sqrt{2}, \\ \{\mathbf{S}\}_{k-1,n} &= \sin\left(\frac{k\pi}{M}\left(n - \frac{N+M}{2}\right)\right), \end{aligned} \quad (17)$$

where $k = 1, 2, \dots, M-1$, and $n = 0, 1, \dots, 2M-1$.

Since the synthesis filters are time-reversed versions of analysis filters, $\mathbf{R}(z)$ can be represented as

$$\mathbf{R}(z) = \mathbf{E}^H(z^{-1}) = [\mathbf{G}_0^H(z^{-2}) \ z\mathbf{G}_1^H(z^{-2})][\mathbf{C}^H \ \mathbf{S}^H]. \quad (18)$$

Substituting (16) and (18), we have

$$\begin{aligned} \mathbf{R}(z)\mathbf{E}(z) &= [\mathbf{G}_0^H(z^{-2}) \ z\mathbf{G}_1^H(z^{-2})][\mathbf{C}^H \ \mathbf{S}^H] \begin{bmatrix} \mathbf{C} \\ \mathbf{S} \end{bmatrix} \\ &\quad \times \begin{bmatrix} \mathbf{G}_0(z^2) \\ z^{-1}\mathbf{G}_1(z^2) \end{bmatrix}. \end{aligned} \quad (19)$$

According to (17), it is derived that $\mathbf{C}^H\mathbf{C} + \mathbf{S}^H\mathbf{S} = M\mathbf{I}_{2M}$. Subsequently we deduce the following theorem.

Theorem: The DTCMFB is a PR system, that is, Eq. (14) holds, if and only if the following conditions are true:

$$G_k(z)G_k^H(z^{-1}) + G_{M+k}(z)G_{M+k}^H(z^{-1}) = 1/M, \quad k = 0, 1, \dots, M-1. \quad (20)$$

It is obvious that the design of DTCMFB is simplified to that of a LP prototype filter, reducing the design complexity significantly. Here it should be pointed out that if the polyphase components $G_k(z)$ in (20) have different orders, some coefficients of prototype filter $p(n)$ will be restricted to 0, which will in turn limit the prototype filter quality. To avoid this, we usually choose the prototype order to be $2m_0M - 1$ in practical design (m_0 is a positive integer), although it can be arbitrary. Please refer to [24] for the detailed description of the choice of prototype filter order.

Recalling that in Section II-B, it was assumed $H_0(z)$ had the stopband edges less than π/M and the stopband responses sufficiently high. In order to perform this assumption and

make $p(n)$ satisfy (20), we minimize the following objective function,

$$\phi = \int_{\frac{\pi}{2M} + \varepsilon}^{\pi} |P(e^{j\omega})|^2 d\omega, \quad 0 < \varepsilon < \pi/2M, \quad (21)$$

under the equality constraints (20). Due to the LP property of $p(n)$ and the conditions (20), the number of free parameters for optimization is one quarter of the number of filter coefficients. This optimization problem has been studied extensively and can be solved by many available algorithms, such as the spectral factorization method [23], second-order cone-programming approach [25], and iterative quadratic programming algorithm [26]. For simplicity, in our simulation we employ the nonlinear optimization function 'fmincon' in MATLAB to perform it.

As an example, a DTCMFB with $M = 3$ and $N = 17$ is considered. Its prototype filter is designed by using the 'fmincon' function in MATLAB. Figs. 7(a)~(d) display the primal and dual analysis filters which are obtained by modulation from the designed prototype filter. It can be seen that all the modulated filters have the symmetric or anti-symmetric impulse responses and thus have the LP property.

Here we would like to point out some remarks on the proposed DTCMFB. Like the conventional DTTs such as DTCWT and DTCWP, the DTCMFB can also have the property of multiresolution. However, its multiresolution decomposition is performed by applying the DTCMFB on lowpass branches iteratively, rather than iterating the primal and dual FBs separately as in Fig. 1(a). This is due to the fact that although DTCMFB is a PR system, neither the primal nor the dual FB is PR. As a result, the redundancy of multiresolution DTCMFB will depend on the number of decomposition levels (The DOECFB [19] has the same limitation). Particularly, the 1D DTCMFB will introduce the redundancy of 2 in each decomposition level. This is different from the DTCWT [2], DTCWP [7] and CSMFB [18] that always have the redundancy of 2 for one-dimensional signals, no matter what the decomposition level is.

IV. DIRECTIONAL-SELECTIVITY OF 2D DTCMFB

The proposed DTCMFB can be extended to two-dimensions via separable filtering along columns and rows followed by an operation of linear combination. And thus the resulting 2D DTCMFB has the redundancy of 4 (generally 2^d in d -dimensions). Without loss of generality, we show the configuration of the k_1 -th channel filtering along columns and the k_2 -th channel filtering along rows in Fig. 8(a), where

$$c_1 = \begin{cases} 2, & k_1 = 0, M, \\ 1, & k_1 = 1, 2, \dots, M-1, \end{cases}$$

and

$$c_2 = \begin{cases} 2, & k_2 = 0, M, \\ 1, & k_2 = 1, 2, \dots, M-1. \end{cases} \quad (22)$$

It can be observed that the separable filtering produces four lowpass subbands and $4((M+1)^2 - 1)$ bandpass subbands.

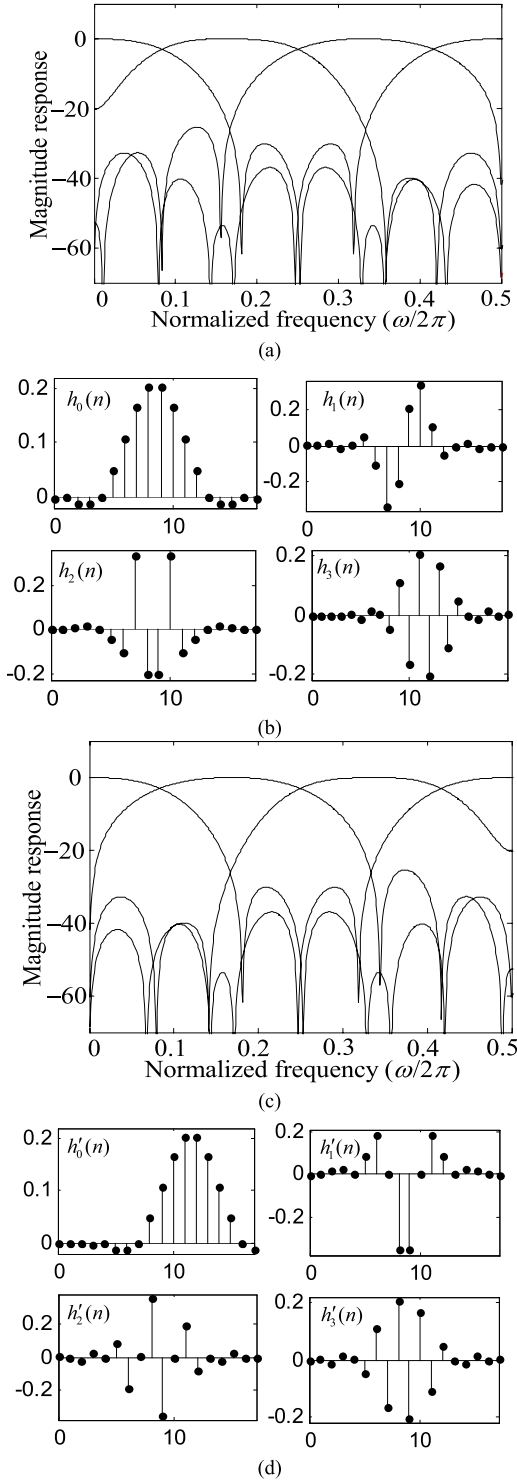


Fig. 7. Design example of a DTCMFB with decimation factor 3 and filter order 17. (a) Normalized magnitude responses of primal analysis filters, (b) impulse responses of primal analysis filters, (c) normalized magnitude responses of dual analysis filters, (d) impulse responses of dual analysis filters.

The spectrum of each bandpass subband occupies four quadrants in the 2D frequency plane $[-\pi, \pi]^2$, leading to poor directional-selectivity.

In order to provide directional-selectivity, the spectrum in the first and third quadrants should be separated from that in

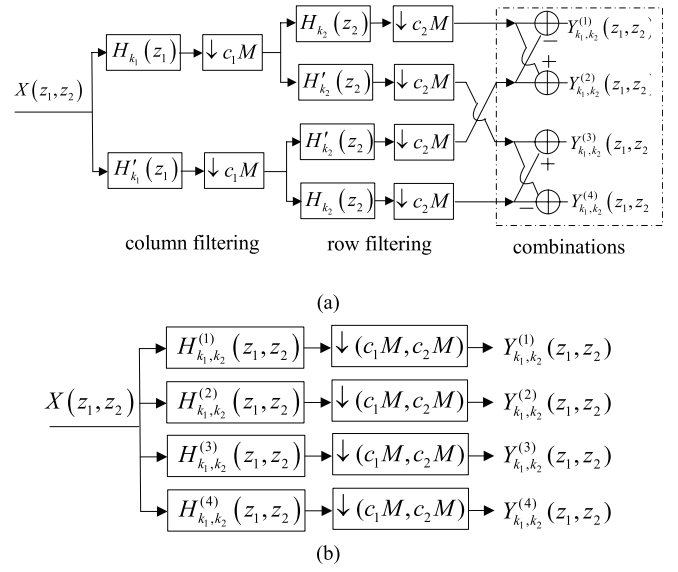


Fig. 8. (a) Configuration of the k_1 -th channel along columns and the k_2 -th channel along rows of the 2D DTCMFB, $k_1, k_2 = 0, 1, \dots, M$, (b) its equivalent structure.

the second and fourth quadrants. This can be performed by linearly combining the bandpass subbands as shown in the dashed box of Fig. 8(a). To analyze the directional-selectivity of the combinations $Y_{k_1, k_2}^{(1)}(z_1, z_2)$, $Y_{k_1, k_2}^{(2)}(z_1, z_2)$, $Y_{k_1, k_2}^{(3)}(z_1, z_2)$ and $Y_{k_1, k_2}^{(4)}(z_1, z_2)$, it is equivalent to analyze the directional-selectivity of their corresponding analysis filters $H_{k_1, k_2}^{(1)}(z_1, z_2)$, $H_{k_1, k_2}^{(2)}(z_1, z_2)$, $H_{k_1, k_2}^{(3)}(z_1, z_2)$ and $H_{k_1, k_2}^{(4)}(z_1, z_2)$ (see Fig. 8(b)), where

$$H_{k_1, k_2}^{(1)}(z_1, z_2) = H_{k_1}(z_1) H_{k_2}(z_2) - H'_{k_1}(z_1) H'_{k_2}(z_2), \quad (23a)$$

$$H_{k_1, k_2}^{(2)}(z_1, z_2) = H_{k_1}(z_1) H_{k_2}(z_2) + H'_{k_1}(z_1) H'_{k_2}(z_2), \quad (23b)$$

$$H_{k_1, k_2}^{(3)}(z_1, z_2) = H'_{k_1}(z_1) H_{k_2}(z_2) + H_{k_1}(z_1) H'_{k_2}(z_2), \quad (23c)$$

$$H_{k_1, k_2}^{(4)}(z_1, z_2) = H'_{k_1}(z_1) H_{k_2}(z_2) - H_{k_1}(z_1) H'_{k_2}(z_2). \quad (23d)$$

Due to the difference between the lowpass (highpass) and bandpass branches, the linear combinations (23) will be considered in the following cases.

Case 1: Lowpass filtering along columns and bandpass filtering along rows.

In this case, we have $k_1 = 0, k_2 = 1, 2, \dots, M-1, c_1 = 2$ and $c_2 = 1$. Substituting (8) and (10) into (23), we obtain

$$\begin{aligned} H_{0, k_2}^{(1)}(z_1, z_2) &= \sqrt{2} e^{-j\left(\frac{\omega_1 M}{2} - \frac{\pi}{4}\right)} P(z_1) \left(\cos\left(\frac{\omega_1 M}{2} - \frac{\pi}{4}\right) a_{k_2} U_{k_2}(z_2) \right. \\ &\quad \left. + j \sin\left(\frac{\omega_1 M}{2} - \frac{\pi}{4}\right) a_{k_2}^* U_{k_2}^*(z_2) \right), \quad (24a) \end{aligned}$$

$$\begin{aligned} H_{0, k_2}^{(2)}(z_1, z_2) &= \sqrt{2} e^{-j\left(\frac{\omega_1 M}{2} + \frac{\pi}{4}\right)} P(z_1) \left(\cos\left(\frac{\omega_1 M}{2} + \frac{\pi}{4}\right) a_{k_2} U_{k_2}(z_2) \right. \\ &\quad \left. + j \sin\left(\frac{\omega_1 M}{2} + \frac{\pi}{4}\right) a_{k_2}^* U_{k_2}^*(z_2) \right), \quad (24b) \end{aligned}$$

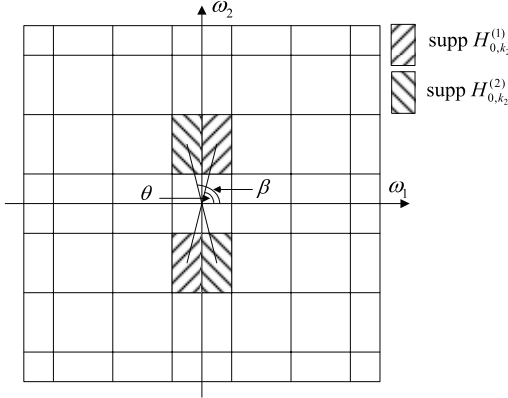


Fig. 9. Sketches of the frequency supports of $H_{0,k_2}^{(1)}(z_1, z_2)$ and $H_{0,k_2}^{(2)}(z_1, z_2)$, where $\theta = \arctan 4k_2$ and $\beta = \pi - \arctan 4k_2$, $k_2 = 1, 2, \dots, M-1$.

$$H_{0,k_2}^{(3)}(z_1, z_2) = \sqrt{2}e^{-j\left(\frac{\omega_1 M}{2} + \frac{\pi}{4}\right)} P(z_1) \left(\cos\left(\frac{\omega_1 M}{2} - \frac{\pi}{4}\right) a_{k_2} U_{k_2}(z_2) - j \sin\left(\frac{\omega_1 M}{2} - \frac{\pi}{4}\right) a_{k_2}^* U_{k_2}^*(z_2) \right), \quad (24c)$$

$$H_{0,k_2}^{(4)}(z_1, z_2) = \sqrt{2}P(z_1) e^{-j\left(\frac{\omega_1 M}{2} - \frac{\pi}{4}\right)} \left(\cos\left(\frac{\omega_1 M}{2} + \frac{\pi}{4}\right) a_{k_2} U_{k_2}(z_2) - j \sin\left(\frac{\omega_1 M}{2} + \frac{\pi}{4}\right) a_{k_2}^* U_{k_2}^*(z_2) \right). \quad (24d)$$

When $\omega_1 \in [0, \pi/2M]$, it can be derived that $\cos(\omega_1 M/2 - \pi/4) \in [1/\sqrt{2}, 1]$ and $\sin(\omega_1 M/2 - \pi/4) \in [-1/\sqrt{2}, 0]$; while for $\omega_1 \in [-\pi/2M, 0]$, $\cos(\omega_1 M/2 - \pi/4) \in [0, 1/\sqrt{2}]$ and $\sin(\omega_1 M/2 - \pi/4) \in [-1, -1/\sqrt{2}]$. Since $P(z_1)$ and $U_{k_2}(z_2)$ have the passbands of $[-\pi/2M, \pi/2M]$ and $[(2k_2 - 1)\pi/2M, (2k_2 + 1)\pi/2M]$, respectively, it can be considered that the frequency support of $H_{0,k_2}^{(1)}(z_1, z_2)$ is $([0, \pi/2M] \times [(2k_2 - 1)\pi/2M, (2k_2 + 1)\pi/2M]) \cup ([-\pi/2M, 0] \times [-(2k_2 + 1)\pi/2M, -(2k_2 - 1)\pi/2M])$ which is located in the first and third quadrants. While that of $H_{0,k_2}^{(2)}(z_1, z_2)$ is $([-\pi/2M, 0] \times [(2k_2 - 1)\pi/2M, (2k_2 + 1)\pi/2M]) \cup ([0, \pi/2M] \times [-(2k_2 + 1)\pi/2M, -(2k_2 - 1)\pi/2M])$ located in the second and fourth quadrants. As illustrated in Fig. 9, both $H_{0,k_2}^{(1)}(z_1, z_2)$ and $H_{0,k_2}^{(2)}(z_1, z_2)$ are directionally selective and are oriented in the direction of $\arctan 4k_2$ and $\pi - \arctan 4k_2$, respectively. From (24) we see that, $H_{0,k_2}^{(3)}(z_1, z_2)$ and $H_{0,k_2}^{(4)}(z_1, z_2)$ have the same frequency supports with $H_{0,k_2}^{(1)}(z_1, z_2)$ and $H_{0,k_2}^{(2)}(z_1, z_2)$, Therefore, they are also directionally selective and have the same directions with $H_{0,k_2}^{(1)}(z_1, z_2)$ and $H_{0,k_2}^{(2)}(z_1, z_2)$, respectively.

Case 2: Highpass filtering along columns and bandpass filtering along rows.

Consider this case, where $k_1 = M$, $k_2 = 1, 2, \dots, M-1$, $c_1 = 2$ and $c_2 = 1$. Since the highpass filters are derived via shifting the lowpass by π (see (8)), it can be analyzed similarly with Case 1 that $H_{M,k_2}^{(1)}(z_1, z_2)$ and $H_{M,k_2}^{(3)}(z_1, z_2)$ have the support

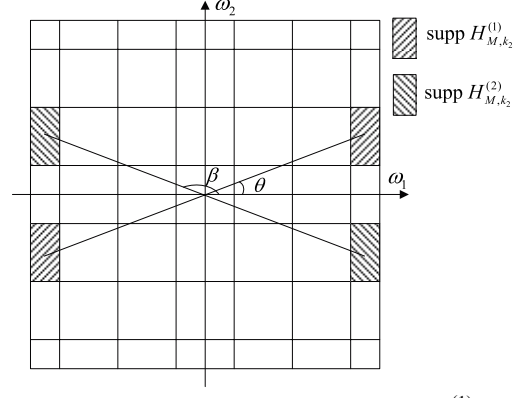


Fig. 10. Sketches of the frequency supports of $H_{M,k_2}^{(1)}(z_1, z_2)$ and $H_{M,k_2}^{(2)}(z_1, z_2)$, where $\theta = \arctan 4k_2/(4M-1)$ and $\beta = \pi - \theta$, $k_2 = 1, 2, \dots, M-1$.

$([\pi - \pi/2M, \pi] \times [(2k_2 - 1)\pi/2M, (2k_2 + 1)\pi/2M]) \cup ([-\pi, -\pi + \pi/2M] \times [-(2k_2 + 1)\pi/2M, -(2k_2 - 1)\pi/2M])$, which is in the first and third quadrants of 2D frequency plane, while $H_{M,k_2}^{(2)}(z_1, z_2)$ and $H_{M,k_2}^{(4)}(z_1, z_2)$ have the frequency support $([-\pi, -\pi + \pi/2M] \times [(2k_2 - 1)\pi/2M, (2k_2 + 1)\pi/2M]) \cup ([\pi, \pi - \pi/2M] \times [-(2k_2 + 1)\pi/2M, -(2k_2 - 1)\pi/2M])$ which is in the second and fourth quadrants (see Fig. 10). Therefore, in this case all the linear combinations have directional-selectivity, where $H_{M,k_2}^{(1)}(z_1, z_2)$ and $H_{M,k_2}^{(3)}(z_1, z_2)$ are oriented in the direction of $\arctan 4k_2/(4M-1)$, and $H_{M,k_2}^{(2)}(z_1, z_2)$ and $H_{M,k_2}^{(4)}(z_1, z_2)$ are oriented in the opposite direction $\pi - \arctan 4k_2/(4M-1)$.

Case 3: Bandpass filtering along both the columns and rows.

In this case, $k_1, k_2 = 1, 2, \dots, M-1$ and $c_1 = c_2 = 1$. Substituting (10) into (23), we have

$$H_{k_1,k_2}^{(1)}(z_1, z_2) = 2a_{k_1} a_{k_2} U_{k_1}(z_1) U_{k_2}(z_2) + 2a_{k_1}^* a_{k_2}^* U_{k_1}^*(z_1) U_{k_2}^*(z_2), \quad (25a)$$

$$H_{k_1,k_2}^{(2)}(z_1, z_2) = 2a_{k_1} a_{k_2}^* U_{k_1}(z_1) U_{k_2}^*(z_2) + 2a_{k_1}^* a_{k_2} U_{k_1}^*(z_1) U_{k_2}(z_2), \quad (25b)$$

$$H_{k_1,k_2}^{(3)}(z_1, z_2) = -2j(a_{k_1} a_{k_2} U_{k_1}(z_1) U_{k_2}(z_2) - a_{k_1}^* a_{k_2}^* U_{k_1}^*(z_1) U_{k_2}^*(z_2)), \quad (25c)$$

$$H_{k_1,k_2}^{(4)}(z_1, z_2) = -2j(a_{k_1} a_{k_2}^* U_{k_1}(z_1) U_{k_2}^*(z_2) - a_{k_1}^* a_{k_2} U_{k_1}^*(z_1) U_{k_2}(z_2)). \quad (25d)$$

According to (9), it is observed that $U_k(z)$ and $U_k^*(z)$ have the passbands of $[(2k-1)\pi/2M, (2k+1)\pi/2M]$ and $[-(2k+1)\pi/2M, -(2k-1)\pi/2M]$, respectively. Thus one can easily derive that, the frequency supports of $H_{k_1,k_2}^{(1)}(z_1, z_2)$ and $H_{k_1,k_2}^{(3)}(z_1, z_2)$ are $([(2k_1-1)\pi/2M, (2k_1+1)\pi/2M] \times [(2k_2-1)\pi/2M, (2k_2+1)\pi/2M]) \cup ([-(2k_1+1)\pi/2M, -(2k_1-1)\pi/2M] \times [-(2k_2+1)\pi/2M, -(2k_2-1)\pi/2M])$ which are strongly oriented at the direction of $\arctan k_2/k_1$, and $H_{k_1,k_2}^{(2)}(z_1, z_2)$ and $H_{k_1,k_2}^{(4)}(z_1, z_2)$ have that of $([(2k_1-1)\pi/2M, (2k_1+1)\pi/2M] \times [-(2k_2+1)\pi/2M, -(2k_2-1)\pi/2M]) \cup ([-(2k_1+1)\pi/2M, -(2k_1-1)\pi/2M] \times [(2k_2-1)\pi/2M,$

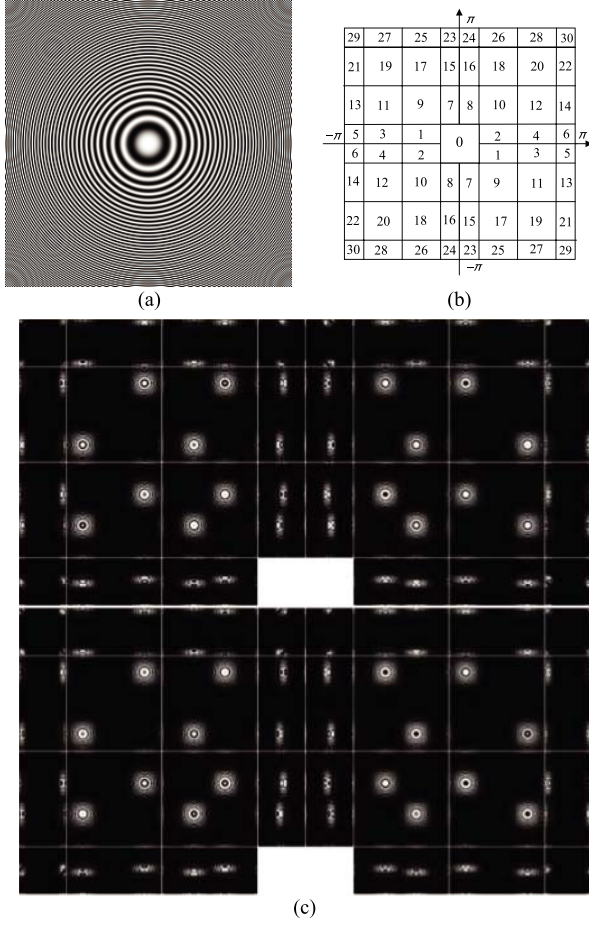


Fig. 11. Example of a 2D DTCMFB with $M = 3$. (a) Original image, (b) frequency partition, (c) directional subbands, where the upper ones are the primal and the lower are the dual.

$(2k_2 + 1)\pi/2M]$ which have the orientation of $\pi - \arctan k_2/k_1$.

From the above analysis, we see that the linear combinations (23) in all the three cases are directionally selective, and the 2D DTCMFB resulting from a 1D DTCMFB with decimation factor M can provide $2((M + 1)^2 - 1)$ directions. Furthermore, with the similar analysis on the shift-invariance of 1D DTCMFB, it is easily found that the aliasing caused by downsampling the output of $H_{k_1, k_2}^{(1)}(z_1, z_2)$ ($H_{k_1, k_2}^{(2)}(z_1, z_2)$) can be cancelled approximately with that caused by downsampling the output of $H_{k_1, k_2}^{(3)}(z_1, z_2)$ ($H_{k_1, k_2}^{(4)}(z_1, z_2)$). Therefore, we here refer to $Y_{k_1, k_2}^{(1)}(z_1, z_2)$ and $Y_{k_1, k_2}^{(2)}(z_1, z_2)$ in Fig. 8 as the primal directional subbands, while $Y_{k_1, k_2}^{(3)}(z_1, z_2)$ and $Y_{k_1, k_2}^{(4)}(z_1, z_2)$ are their corresponding dual directional subbands. Since $H_{k_1, k_2}^{(3)}(z_1, z_2)$ and $H_{k_1, k_2}^{(4)}(z_1, z_2)$ have the same frequency supports with $H_{k_1, k_2}^{(1)}(z_1, z_2)$ and $H_{k_1, k_2}^{(2)}(z_1, z_2)$, all the dual directional subbands have the same directions with the corresponding primal directional ones. Note that similar with 1D DTCMFB, the 2D DTCMFB can perform the multiresolution decomposition by iterating the lowpass subbands, and will introduce the redundancy of 4 in each decomposition level.

To illustrate the flexible directional-selectivity, we employ a single-level 2D DTCMFB with $M = 3$ to decompose

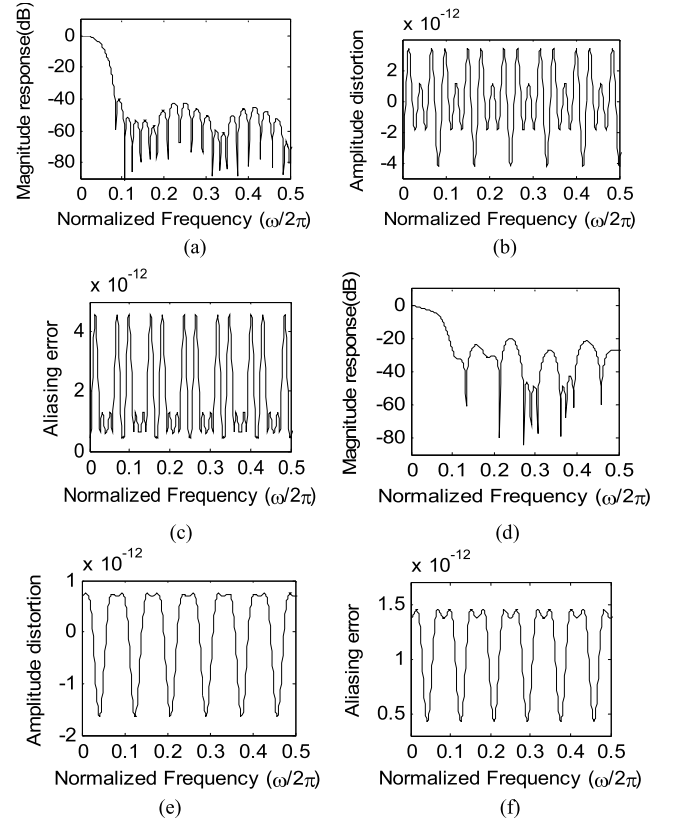


Fig. 12. Comparison of the proposed DTCMFB and DOECFB [19] with $M = 6$. (a) Prototype magnitude response of DTCMFB, (b) amplitude distortion of DTCMFB, (c) aliasing error of DTCMFB, (d) prototype magnitude response of DOECFB, (e) amplitude distortion of DOECFB, (f) aliasing error of DOECFB.

the test image *Zoneplate* (see Fig. 11(a)), for its frequency contents occupy the whole 2D frequency plane $[-\pi, \pi]^2$. The frequency partition scheme of the 2D DTCMFB is shown in Fig. 11(b). This is different from the DOECFB [19] in which the primal lowpass and highpass filters have no corresponding dual, mixing some directional subbands together, such as the ones 13 and 14, and the ones 15 and 16. According to Fig. 11(b), the image *Zoneplate* is decomposed into four lowpass, thirty primal and thirty dual directional subbands. Fig. 11(c) displays these directional subbands, where the upper ones are the primal and the lower ones are the dual. From this example, it is obvious that 2D DTCMFB can provide higher directional-selectivity and thus has the potential to represent the images with abundant directional features.

V. SIMULATION RESULTS

In this section, firstly we give several examples to test the performances of reconstruction and shift-invariance of the proposed DTCMFB. Then we apply the 2D DTCMFB to nonlinear approximation (NLA) and image denoising to verify its potential in image processing.

A. Evaluation of Reconstruction Performance

This subsection considers a DTCMFB with $M = 6$. Its prototype filter $p(n)$ with the specifications given in Table I is firstly designed by minimizing the object function (21) under the PR constraints (20). Fig. 12(a) shows the magnitude

TABLE I
SPECIFICATIONS OF THE PROTOTYPE FILTERS FOR DOECFB AND DTCMFB USED IN EVALUATION OF RECONSTRUCTION PERFORMANCE

Specifications	Filter order	Zero coefficients	Free parameters	Stopband attenuation
For DOECFB	54	21	9	21dB
For DTCMFB	47	0	12	40dB

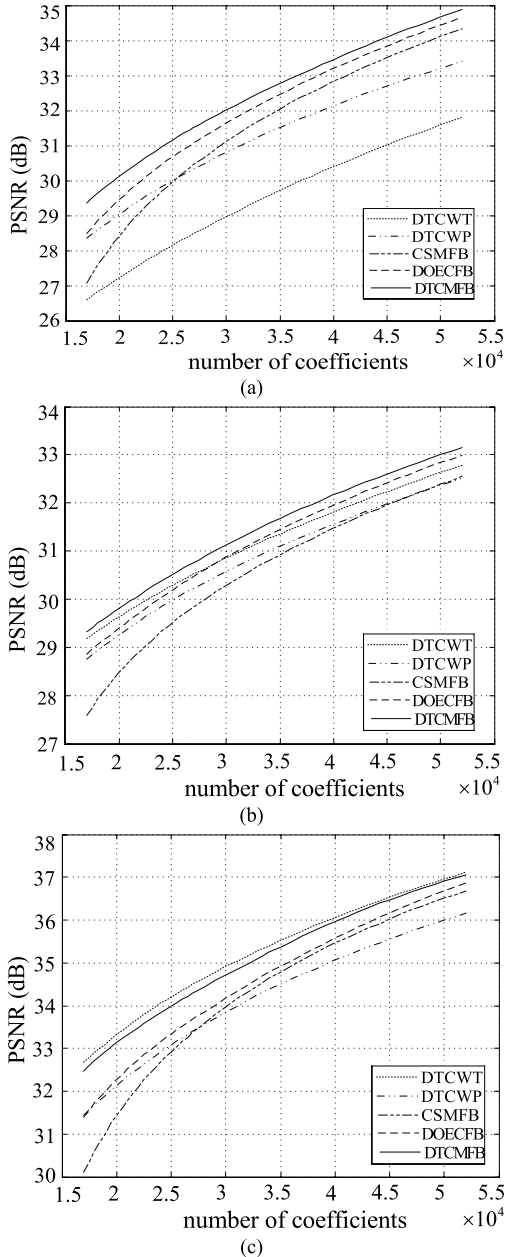


Fig. 13. Nonlinear approximation results. (a) Barbara. (b) Goldhill. (c) Lena.

response of the designed prototype. As for the reconstruction performance of DTCMFB, we use the maximum peak to peak ripple of the amplitude distortion $|A_0(z)|$, denoted by E_{pp} , and the maximum value of the aliasing errors $\sqrt{\sum_{l=1}^{M-1} |A_l(z)|^2}$, denoted by E_a , to evaluate it [23], where $A_0(z)$ and $A_l(z)$ are given in (13). Figs. 12(b) and (c) show the amplitude distortion with $E_{pp} = 7.62 \times 10^{-12}$ and the aliasing error

with $E_a = 4.58 \times 10^{-12}$, respectively. It is obvious that the proposed DTCMFB is a PR system.

For a comparison, we also design a DOECFB [19] with $M = 6$. The order of its prototype filter is set to be 54, which satisfies the constraint of odd multiple of M . Fig. 12(d) shows the magnitude response of this prototype. The amplitude distortion and aliasing error are displayed in Figs. 12(e) and (f), respectively. From Table I we see that, although the prototype of DOECFB has longer order (54 versus 47), its stopband attenuation is much lower than that of the prototype of DTCMFB (21dB versus 40dB). This is because that in the DOECFB, the order constraint together with the PR condition requires 21 coefficients of prototype to be zero and the free parameters for optimization is only 9, reducing the filter quality significantly.

B. Test of Shift-Invariance

To evaluate the shift-invariance of DTCMFB, this subsection will employ a single-level DTCMFB with $M = 8$ and compare its shift-invariance with those of a 3-level DTCWP [7] and a single-level DOECFB with $M = 8$ [19]. For a 3-level DTCWP, both its primal and dual FBs have 2^3 equivalent channels and the equivalent decimation factor 2^3 . The involved filters of the 3-level DTCWP are from the website <http://www2.itu.edu.tr/~ibayram/>. Since the analysis filters in each level have the order of about 12, it can be derived that those of the equivalent analysis filters are about 80. Therefore, for a fair comparison, the prototype orders of DOECFB and DTCMFB are set to be 88 and 79, respectively. Both of them are designed by using the 'fmincon' function in MATLAB.

Given a FB, its shift-invariance is usually evaluated by the ratio of the total energy of unwanted aliasing transfer functions to the energy of wanted transfer function [2]. Here we give the formulation to calculate these energy ratios R_k for DTCWP, DOECFB and DTCMFB, where

$$R_k = \frac{\sum_{l=1}^{D_k-1} \varepsilon \{H_k(zW_{cM}^l) F_k(z) + H'_k(zW_{cM}^l) F'_k(z)\}}{\varepsilon \{H_k(z) F_k(z) + H'_k(z) F'_k(z)\}} \quad (26)$$

$\varepsilon\{\cdot\}$ calculates the energy, k is the channel index, and D_k is the decimation factor of the k -th channel. Note that since the lowpass and highpass channels of DOECFB have no dual, the energy ratios of the two channels are $\sum_{l=1}^{D_k-1} \varepsilon \{H_k(zW_{cM}^l) F_k(z)\} / \varepsilon \{H_k(z) F_k(z)\}$, $k = 0, M$, but not as in (26). Table II displays the comparison results of energy ratios of DTCWP, DOECFB and DTCMFB. For convenience, we represent R_k in dB by using $10 \log_{10} R_k$. Since the DTCMFB design avoids the fractional-delay constraints encountered in DTCWP, and moreover its prototype has higher

TABLE II
ALIASING ENERGY RATIOS IN DB FOR DTCMFB, DTCWP AND DOECFB

Channel number	$k=0$	$k=1$	$k=2$	$k=3$	$k=4$	$k=5$	$k=6$	$k=7$	$k=8$
DTCWP	-29.55	-22.18	-13.91	-14.06	-29.55	-22.18	-13.91	-14.06	
DOECFB	-15.06	-14.39	-15.05	-15.03	-15.03	-15.03	-15.05	-14.39	-15.06
DTCMFB	-45.44	-45.46	-47.60	-45.66	-45.44	-45.66	-47.60	-45.46	-45.44

TABLE III
REDUNDANCY RATIOS OF THE TRANSFORMS USED IN IMAGE DENOISING SIMULATION

Transforms	DTCWT	DTCWP	5-level Curvelet	CSMFB	2-level DOECFB	1-level DOECFB	2-level DTCMFB	1-level DTCMFB
Redundancy ratio	4	4	7.2	4	4.2	4	4.2	4

filter quality than that of DOECFB, the proposed DTCMFB provides much better shift-invariant performance than both of them.

C. Nonlinear Approximation

This subsection considers the NLA performance of the proposed DTCMFB and compares it with those of the DTCWT [2], DTCWP [7], CSMFB [18] and DOECFB [19]. The employed DTCMFB, CSMFB and DOECFB have the decimation factor 9 and the decomposition level 1. As for DTCWT and DTCWP, we set their decomposition levels to be 5 and 4, respectively. In spite of different decomposition levels, the DTCWT, DTCWP and CSMFB have the same redundancy of 4 (the test signals are two-dimensional images). Due to the single-level decomposition, the redundancy of DOECFB and DTCMFB is also 4. In this simulation, the DTCWT uses the ‘9-7’ and ‘qshift_06’ filters [2] and the filters in DTCWP are from <http://www2.itu.edu.tr/~ibayram/>. Based on the discussion of the choice of prototype filter order in the previous subsection, we set the prototype orders of CSMFB, DOECFB and DTCMFB as 53, 63 and 53, respectively, and then design them using the ‘fmincon’ function in MATLAB.

The 8-bit grayscale images *Barbara*, *Goldhill*, and *Lena* are used for test images, of which *Barbara* and *Goldhill* contain abundant textures and details, while *Lena* has many smooth regions and contours. Their NLA results in peak signal-to-noise ratio (PSNR) by using DTCWT, DTCWP, CSMFB, DOECFB and DTCMFB with different number of retained coefficients are given in Fig. 13. It is obvious that, the proposed DTCMFB outperforms DTCWT and DTCWP consistently on the images *Barbara* and *Goldhill*. Particularly for *Barbara*, the average PSNR gains are 3.00dB over DTCWT and 1.23dB over DTCWP. In the case of the image *Lena* with many smooth regions and contours, the DTCMFB also provides comparable NLA results to DTCWT. Comparing with CSMFB and DOECFB which have the same decimation factor and decomposition level with DTCMFB, since LP filters can preserve the image edge information better than the non-LP filters, the DTCMFB gives better NLA results than CSMFB; in spite of DOECFB having LP filters, the DTCMFB still provides better NLA performance for its good filter quality and flexible directional-selectivity.

Furthermore, we illustrate the zoom-in part of the reconstructed image *Barbara* in Fig. 14 with 16986 coefficients kept. One can observe that in Figs. 14(b) and (d), some texture details are smoothed out (see the scarf of *Barbara*), and in Figs. 14(c) and (e) there are some artifacts in the smooth regions (see the top left part). However in Fig. 14(f), the texture details are well preserved and the artifacts in smooth regions are also reduced. Consequently, we conclude that the proposed DTCMFB gives better visual quality as well as the higher PSNR.

D. Image Denoising

A good NLA performance of a transform often indicates that this transform has potential in many signal/image processing applications [1], such as denoising and feature extraction. Taking the image denoising as an example, we test the commonly used images *Lena*, *Peppers*, *Barbara* and *Zebra* which are shown in Fig. 15. It is clear that *Lena* and *Peppers* are composed of smooth regions and contours, while *Barbara* and *Zebra* contain a lot of textures. All the test images are corrupted with simulated additive zero-mean white Gaussian noise at various noise levels. For the noisy images *Lena* and *Peppers*, we use a 2-level DTCMFB with decimation factor $M = 4$ and filter order $N = 23$ to denoise them, while a single-level DTCMFB with $M = 8$ and $N = 47$ to denoise the noisy *Barbara* and *Zebra*. To highlight the denoising efficiency of DTCMFB, a simple hard-thresholding scheme is employed and the threshold is selected as

$$T_{i,j} = K_i \delta_{i,j}, \quad (27)$$

where K_i is a constant at the i -th decomposition scale, and $\delta_{i,j}$ denotes the noise variance at the j -th directional subband of scale i . The constant K_i is determined by experiment to ensure the optimal denoising performance. The variance $\delta_{i,j}$ is estimated by using Monte-Carlo simulations [27].

For a comparison, we employ the DTTs of DTCWT [2], DTCWP [7], CSMFB [18] and DOECFB [19] to recover the original images from the noisy ones. The decomposition level of DTCWT is set to be 5 for the four test images, while that of DTCWP is 3 for *Lena* and *Peppers* and 4 for *Barbara* and *Zebra*. The filters involved in the DTCWT and DTCWP are chosen to be the same as those used in the NLA

TABLE IV
PSNR VALUES OF THE DENOISING EXPERIMENTS (dB)

	σ PSNR	10	15	20	25	30	35	40	50
		28.13	24.61	22.11	20.17	18.59	17.24	16.09	14.15
<i>Lena</i>	DTCWT	34.50	32.91	31.71	30.74	29.89	29.16	28.56	27.53
	DTCWP	34.50	32.75	31.41	30.33	29.47	28.71	28.05	26.88
	Curvelet	34.68	32.97	31.66	30.68	29.83	29.11	28.52	27.48
	CSMFB	34.41	32.71	31.50	30.52	29.77	29.07	28.47	27.40
	DOECFB	34.39	32.69	31.51	30.48	29.70	28.99	28.46	27.42
	DTCMFB	34.66	32.91	31.71	30.74	29.87	29.17	28.58	27.45
<i>Peppers</i>	DTCWT	33.74	32.33	31.21	30.28	29.51	28.79	28.14	27.06
	DTCWP	33.57	32.13	30.98	29.96	29.15	28.32	27.64	26.53
	Curvelet	33.77	32.35	31.28	30.42	29.67	28.95	28.34	27.33
	CSMFB	33.61	31.20	31.05	30.05	29.18	28.47	27.90	26.91
	DOECFB	33.62	32.17	31.02	30.05	29.24	28.44	27.82	26.62
	DTCMFB	33.77	32.42	31.39	30.42	29.65	29.02	28.45	27.42
<i>Barbara</i>	DTCWT	32.70	30.31	28.61	27.31	26.24	25.42	24.71	23.56
	DTCWP	33.58	31.47	29.96	28.79	27.81	27.01	26.28	25.06
	Curvelet	33.44	31.35	29.95	28.86	27.92	27.13	26.46	25.31
	CSMFB	33.61	31.66	30.21	29.05	28.14	27.35	26.66	25.63
	DOECFB	33.59	31.63	30.20	29.07	28.07	27.24	26.48	25.18
	DTCMFB	33.61	31.69	30.26	29.14	28.24	27.44	26.75	25.60
<i>Zebra</i>	DTCWT	34.82	32.15	30.26	28.73	27.49	26.53	25.55	24.09
	DTCWP	34.92	32.36	30.60	29.17	28.07	27.04	26.24	24.82
	Curvelet	34.71	32.09	30.30	28.95	27.83	26.98	26.19	24.94
	CSMFB	34.83	32.30	30.63	29.30	28.15	27.30	26.58	25.27
	DOECFB	35.15	32.60	30.78	29.44	28.31	27.39	26.60	25.23
	DTCMFB	35.17	32.67	30.84	29.52	28.40	27.45	26.63	25.27



Fig. 14. Examples of NLA for the image *Barbara* with 16986 coefficients kept. (a) Original image, (b) DTCWT, PSNR = 26.60dB, (c) DTCWP, PSNR = 28.35dB, (d) CSMFB, PSNR = 27.06dB, (e) DOECFB, PSNR = 28.48dB, (f) DTCMFB, PSNR = 29.38dB.

simulation. As for CSMFB and DOECFB, we set them to have the same decimation factors and decomposition levels with the employed DTCMFB. Moreover, the prototype filter orders of CSMFB are also chosen to be the same as those of

DTCMFB, and those of DOECFB are set as 28 for $M = 4$ and 56 for $M = 8$. All the DTTs have the comparable redundancies as listed in Table III. Table IV summarizes their denoising results at different noise levels. It is obvious the employed

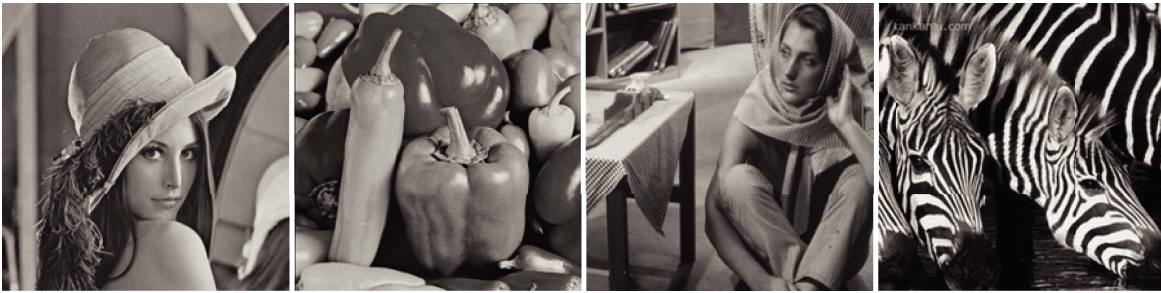


Fig. 15. Original images. From left to right: *Lena*, *Peppers*, *Barbara* and *Zebra*.

DTCMFB yields better denoising results than DTCWT and DTCWP for *Barbara* and *Zebra*. The average improvement is up to 1.26dB over DTCWT and 0.34dB over DTCWP. In the case of *Lena* and *Peppers*, the proposed DTCMFB provides comparable PSNR values to DTCWT. Despite the same decimation factor and decomposition level, the proposed DTCMFB provides higher denoising performance consistently than CSMFB and DOECFB for all the test images. These results are consistent with the NLA performances as shown in Fig. 13.

Furthermore, we compare the denoising results of DTCMFB with those of Curvelet [27], which is suited to represent the curves and contours of images. The multiresolution level of Curvelet is set to be 5, and the directional decompositions levels are set as {3, 4, 4, 5, 5} from the coarsest to the finest scale. Similar with DTTs, the employed Curvelet has the property of shift-invariance, but with a higher redundancy ratio (see Table III). From the experiment results in Table IV one can see that, the proposed DTCMFB outperforms Curvelet consistently for the high-frequency textured images *Barbara* and *Zebra*. The average PSNR gains are 0.29dB for *Barbara* and 0.50dB for *Zebra*. In the case of *Lena* and *Peppers* which have many smooth regions and contours, the DTCMFB also offers comparable or slightly higher PSNR values.

VI. CONCLUSION

In this work, we constructed the DTCMFB, in which both the primal and dual FBs are obtained by cosine-modulating one prototype filter. In addition to shift-invariance, the DTCMFB avoids the fractional-delay constraints during its design and moreover has the LP analysis/synthesis filters which is highly desired in image processing applications. By extending such DTCMFB to two-dimensions, the resulting 2D DTCMFB provides high directional-selectivity, which can decorrelate the prominent features in images flexibly. The experiments on NLA and image denoising have demonstrated its potential power in image processing.

REFERENCES

- [1] S. Mallat, *A Wavelet Tour of Signal Processing: The Sparse Way*, 3rd ed. New York, NY, USA: Academic, 2009.
- [2] N. G. Kingsbury, "Complex wavelets for shift invariant analysis and filtering of signals," *Analysis*, vol. 10, no. 3, pp. 234–253, May 2001.
- [3] I. W. Selesnick, R. G. Baraniuk, and N. G. Kingsbury, "The dual-tree complex wavelet transform," *IEEE Signal Process. Mag.*, vol. 22, no. 6, pp. 123–151, Nov. 2005.
- [4] K. N. Chaudhury and M. Unser, "On the shiftability of dual-tree complex wavelet transforms," *IEEE Trans. Signal Process.*, vol. 58, no. 1, pp. 221–232, Jan. 2010.
- [5] K. N. Chaudhury and M. Unser, "On the Hilbert transform of wavelets," *IEEE Trans. Signal Process.*, vol. 59, no. 4, pp. 1890–1894, Apr. 2011.
- [6] C. Chaux, L. Duval, and J. C. Pesquet, "Image analysis using a dual-tree M-band wavelet transform," *IEEE Trans. Image Process.*, vol. 15, no. 8, pp. 2397–2412, May 2006.
- [7] I. Bayram and I. W. Selesnick, "On the dual-tree complex wavelet packet and M-band transforms," *IEEE Trans. Signal Process.*, vol. 56, no. 6, pp. 2298–2310, Jun. 2008.
- [8] I. W. Selesnick, "The double-density dual-tree DWT," *IEEE Trans. Signal Process.*, vol. 52, no. 5, pp. 1304–1314, May 2004.
- [9] T. T. Nguyen and S. Orintara, "The shiftable complex directional pyramid—Part I: Theoretical aspects," *IEEE Trans. Signal Process.*, vol. 56, no. 10, pp. 4651–4660, Oct. 2008.
- [10] T. T. Nguyen and S. Orintara, "The shiftable complex directional pyramid—Part II: Implementation and applications," *IEEE Trans. Signal Process.*, vol. 56, no. 10, pp. 4661–4672, Oct. 2008.
- [11] K. N. Narayan and M. Unser, "Construction of Hilbert transform pairs of wavelet bases and Gabor-like transforms," *IEEE Trans. Signal Process.*, vol. 57, no. 9, pp. 3411–3425, Sep. 2009.
- [12] L. Y. Wei and T. Blu, "A new non-redundant complex Hilbert wavelet transforms," in *Proc. IEEE Stat. Signal Process. Workshop*, Aug. 2012, pp. 652–655.
- [13] J. Magarey and N. Kingsbury, "Motion estimation using a complex-valued wavelet transform," *IEEE Trans. Signal Process.*, vol. 46, no. 4, pp. 1069–1084, Apr. 1998.
- [14] C. C. Liu and D. Q. Dai, "Face recognition using dual-tree complex wavelet features," *IEEE Trans. Image Process.*, vol. 18, no. 11, pp. 2593–2599, Nov. 2009.
- [15] M. Miller and N. G. Kingsbury, "Image denoising using derotated complex wavelet coefficients," *IEEE Trans. Image Process.*, vol. 17, no. 9, pp. 1500–1511, Sep. 2008.
- [16] J. J. Ranjani and S. J. Thiruvengadam, "Dual-tree complex wavelet transform based SAR despeckling using interscale dependence," *IEEE Trans. Geosci. Remote Sens.*, vol. 48, no. 6, pp. 2723–2731, Jun. 2010.
- [17] T. D. Tran, R. L. de Queiroz, and T. Q. Nguyen, "Linear-phase perfect reconstruction filter bank: Lattice structure, design, and application in image coding," *IEEE Trans. Signal Process.*, vol. 48, no. 1, pp. 133–147, Jan. 2000.
- [18] S. Kyochi, T. Uto, and M. Ikehara, "Dual-tree complex wavelet transform arising from cosine-sine modulated filter banks," in *Proc. IEEE Int. Symp. Circuits Syst.*, May 2009, pp. 2189–2192.
- [19] S. Kyochi and M. Ikehara, "A class of near shift-invariant and orientation-selective transform based on delay-less oversampled even-stacked cosine-modulated filter banks," *IEICE Trans. Fundam. Electron., Commun. Comput.*, vol. E93-A, no. 4, pp. 724–733, Apr. 2010.
- [20] A. Viholainen, T. H. Stitz, J. Alhava, T. Ihalainen, and M. Renfors, "Complex modulated critically sampled filter banks based on cosine and sine modulation," in *Proc. IEEE Int. Symp. Circuits Syst.*, vol. 1, May 2002, pp. 833–836.
- [21] Y. P. Lin and P. P. Vaidyanathan, "Linear phase cosine modulated maximally decimated filter banks with perfect reconstruction," *IEEE Trans. Signal Process.*, vol. 42, no. 11, pp. 2525–2539, Nov. 1995.
- [22] H. Bolcskei and F. Hlawatsch, "Oversampled cosine modulated filter banks with perfect reconstruction," *IEEE Trans. Circuits Syst. II, Analog Digit. Signal Process.*, vol. 45, no. 8, pp. 1057–1071, Aug. 1998.
- [23] P. P. Vaidyanathan, *Multirate System and Filter Banks*. Englewood Cliffs, NJ, USA: Prentice-Hall, 1993.

- [24] T. Q. Nguyen and R. D. Koilpillai, "The theory and design of arbitrary-length cosine-modulated filter banks and wavelets, satisfying perfect reconstruction," *IEEE Trans. Signal Process.*, vol. 44, no. 3, pp. 473–483, Mar. 1996.
- [25] W. S. Lu, T. Saramaki, and R. Bregovic, "Design of practically perfect-reconstruction cosine-modulated filter banks: A second-order cone programming approach," *IEEE Trans. Circuits Syst. I, Reg. Papers*, vol. 51, no. 3, pp. 552–563, Mar. 2004.
- [26] G. Doblinger, "A fast design method for perfect-reconstruction uniform cosine-modulated filter banks," *IEEE Trans. Signal Process.*, vol. 60, no. 12, pp. 6693–6697, Dec. 2012.
- [27] J. L. Starck, E. J. Candes, and D. L. Donoho, "The curvelet transform for image denoising," *IEEE Trans. Image Process.*, vol. 11, no. 6, pp. 670–684, Jun. 2002.



Han Liu received the B.S. degree in automation from the Shannxi Mechanical Institute, Xi'an, China, in 1993, and the M.S. and Ph.D. degrees in control science and engineering from the Xi'an University of Technology, Xi'an, in 1996 and 2003, respectively. He is currently a Professor and the Dean with the Faculty of Automation and Information Engineering, Xi'an University of Technology. His current research interests include pattern recognition, intelligent information processing, and nonlinear system control.



Lili Liang received the B.S. degree in electronic information engineering from the Xi'an University of Technology, Xi'an, China, in 2005 and the Ph.D. degree in circuits and system from Xi'dian University, Xi'an, in 2012. Since April 2012, she has been a Lecturer with the Xi'an University of Technology. Her research interests are in the areas of multirate signal processing, multidimensional filter bank, and sparse image representation.